Photoelastic Observation of Microscopic Force Transmission in Granular Material with Fabric Change

Richard Wan[1], Al-Mamun[2] and Peijun Guo[3]

Abstract

The roles of dilatancy and fabric on the behavior of granular materials are both numerically and experimentally explored for the study of material instability and failure. This investigation has two basic ingredients: namely a stress dilatancy model with embedded microstructural information through a fabric tensor, and an experimental rendition of force transmission and structure in an assembly of 2D photoelastic disks. In order to highlight material instability, model simulations of sand behavior are carried out in triaxial stress conditions along proportional strain paths with varying degrees of controlled dilation (or compaction) including isochoric deformations as a particular case. It is shown that a dense sand can succumb to instability or liquefaction in other than isochoric (undrained) conditions. Photoelastic observations reveal that this instability is highly dependent on microscopic features such as particle geometry, packing, and diameter among others.

Key Words: Fabric; Dilatancy; Photoelasticity; Force chains; Strain paths; Stress paths

Introduction

The behavior of granular materials such as sands is controlled by their dilatancy and the mode by which the applied stresses are carried by so-called force chains. It is because of the discrete nature of the system that dilatancy manifests itself through geometrical grain rearrangements with the fabric acting as a constraint against applied stresses. Therefore, in the pursuit of fundamentals, it is pertinent to study fabric in sand and systematically incorporate it in any constitutive modeling endeavor for the analysis of failure, material instability as well as strain localization.

Stress dilatancy theories have been traditionally developed for soils based on macroscopic analysis through energy principles (e.g., Rowe 1962). However, incorporating micro- or meso-scale phenomenon in a continuum model is a challenging task since any theory developed is difficult to completely verify, given that experimental data on fabric is scarce (Oda and Iwashita 1999). For instance, micro/meso-macro relationships give way to a mathematical description of fabric and its relationship to stresses and deformations, but its evolution with deformation history remains elusive without experimental data. Micro-mechanical pursuits of stress dilatancy description exist in the literature; to name a few, see Matsuoka & Takeda (1980), Nemat-Nasser (2000), Wan & Guo (2001).

In this study, we use the model developed by Wan & Guo (2001) with an embedded fabric-dependent dilatancy rule in order to illustrate the central roles of dilatancy and fabric on material stability along imposed strain paths, rather than stress paths. By controlling volume changes in a particular manner during deformation history, we demonstrate that a dense sand can succumb to instability or liquefaction in other than isochoric (undrained) conditions. On the other hand, force chains revealed during the biaxial loading of an assembly of photoelastic disks help to understand the failure mechanism leading to unstable behavior and role of fabric.

Received 30 January 2004, Accepted 14 July 2004

[1]Associate Professor, Department of Civil Engineering, University of Calgary, AB T2N 1N4, Canada

[2]Graduate Student, Department of Civil Engineering, University of Calgary, AB T2N 1N4, Canada
Email: mamalmam@ucalgary.ca

[3]Assistant Professor, Department of Civil Engineering, McMaster University, Hamilton, ONT L8S 4L7, Canada

This study touches upon the understanding of flow in granular materials, soil-structure interaction problems under extreme loading conditions, as well as slope stability problems with pre-shear small perturbations.

Fabric-Embedded Dilatancy Model

We begin with a brief recapitulation of the model essentials for describing fabric dependencies through a micro-mechanical analysis that involves equating the total energy dissipation of a grain assembly endowed with some fabric to the total work input, Guo (2000). The stress-dilatancy equation that emerges from such an analysis can be expressed in axi-symmetric stress and strain conditions after some simplifications as follows:

$$\frac{\dot{\varepsilon}_v}{\dot{\gamma}} = -\frac{4}{3}\frac{(\sin\varphi_f - \sin\varphi_m)}{(1-\sin\varphi_f \sin\varphi_m)} \tag{1}$$

Where, $\dot{\varepsilon}_v$ = plastic volumetric strain rate, $\dot{\gamma}$ = plastic shear strain rate, φ_m = mobilized friction angle, and φ_f = characteristic friction angle. It is interesting to note that Eq. (1) takes the same form as the standard Rowe's dilatancy equation, except for a characteristic friction herein introduced that establishes the link to fabric, i.e.

$$\sin\varphi_f = \frac{X(F_{33}/F_{11}) + \gamma^*}{a + \gamma^*}\left(\frac{e}{e_{cr}}\right)^{\alpha} \sin\varphi_{cv} \tag{2}$$

Where, e and e_{cr} are current and critical void ratios respectively, φ_{cv} is the friction angle at critical state, while X, a and α are constants. Fabric information is transmitted through fabric components F_{11} and F_{33} which are projections of the second order fabric tensor F_{ij} (Wan & Guo 2001) along principal stress directions σ_1 and σ_3 respectively, and the transformed plastic shear strain term γ^* which factors conventional strain with fabric. In general, fabric and stress tensors are not coaxial.

It is evident from Eq. (1) that both positive and negative rates of dilation can be obtained depending on the relative magnitudes of φ_m and φ_f. In the limit, fabric conditions can be such that a positive rate of dilation is possible even though the current void ratio is looser of critical, i.e. $e > e_{cr}$.

Setting aside all details of constitutive modeling derivations, the stress dilatancy described in Eq. (1) has been used as a

flow rule in a double hardening elasto-plastic model (Wan & Guo 2001). Apart from describing plastic hardening via mobilized friction angle, a fabric evolution law needs to be established as follows:

$$\dot{F}_{ij} = \chi \, \dot{\eta}_{ij}; \quad \eta_{ij} = \frac{s_{ij}}{p} \tag{3}$$

which intimates that fabric component changes ($\dot{F}_{ij}$) are purely deviatoric and coaxial with the rate of change of deviatoric stress ratio tensor $\eta_{ij} = s_{ij}/p$; with s_{ij} = deviatoric stress and p = mean stress.

Fig. 1 shows a family of energy dissipation curves plotted as applied stress ratio (σ_1/σ_3) against dilatancy rates $D = (1-\dot{\varepsilon}_1/\dot{\varepsilon}_v)$calculated by the model for the case of loose (e_0 = 0.65) Ottawa sand with fixed initial anisotropy (fabric ratio $\Omega = F_1/F_3 = 1.33$; F_1 and F_3 being major and minor principal fabrics respectively) but with varying bedding planes in which grain contact normals are dominant. It is found that with increasing bedding angle, the initial dilation rate decreases, i.e., the sample undergoes more volumetric compaction initially, while the maximum dilatancy and the corresponding mobilized stress ratio (i.e., the maximum one) decrease. Basically, the higher the bedding angle, the higher the threshold stress ratio at which the compaction-dilation transition occurs.

Imposed Proportional Strain Paths

The response of sand along proportional strain paths with constant deformation rate $\vartheta = d\varepsilon_v/d\gamma$ is examined. As such, the standard undrained test corresponds to $\vartheta = 0$, while constant compaction and dilation rate tests refer to positive and negative ϑ's respectively. Strain path controlled experimental studies are scarce in the literature, with the exception of the work reported by Chu et al. (1992) that probe sand behavior along proportional strain paths with reference to strain softening and localization - viz. material stability. From a practical viewpoint, Vaid and Sivathayalan (2000) have also investigated strain path tests by controlling the drainage conditions in the test specimen since water flowing into or out of it would cause either dilation or contraction. The rationale of such tests is that under real field situations, soils deform in a partially drained condition.

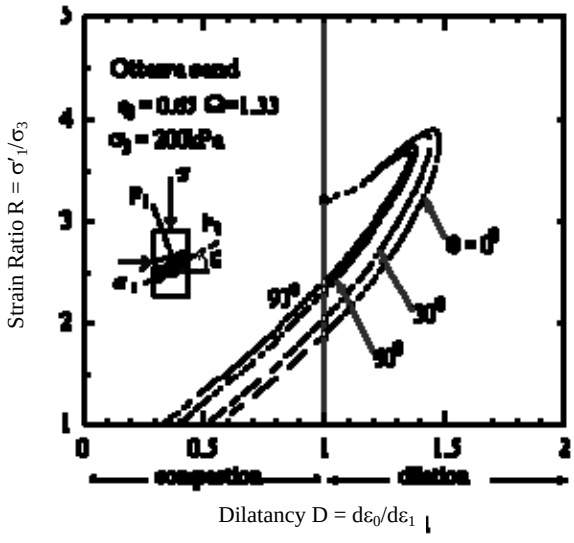

Fig. 1 Stress dilatancy curves as a function of initial fabric

Model Simulations

With this brief overview, we now turn to model simulations of Fig. 2 pertaining to the behavior of dense (e_0 = 0.60) Ottawa sand along a variety of proportional strain paths ϑ (–3.0 to +1.0) at an initial confining pressure of 200 kPa. In this set of calculations, the initial fabric was assumed to be isotropic, but evolved subsequently during deformation history. It is found that the sand displays stable behavior for positive ϑ's, including the undrained case. By stable behavior, we mean that the second order work $d^2W = d\sigma.d\varepsilon$ is positive (Hill 1959). On the other hand, for largely negative ϑ's referring to forced dilation on the specimen, the effective stress path displays unstable response just like for a loose sand under undrained conditions. Thus, the material strength associated with any proportional strain path is not bounded by the undrained and drained conditions as shown in Fig. 2. It would be then erroneous to derive material strength solely based on undrained conditions.

Fig. 2 shows a peculiar stress path for ϑ = –0.15 which displays an initial hardening (stable) phase ABC, terminating into an unstable one with a snap-back at C. Fig. 3 compares the stress path with the one obtained for the same ϑ value, but with an initial fabric ratio $\Omega = F_1/F_3$ of 1.33. The higher deviatoric stress q sustained by the soil for the latter case is understandable, given that the initial anisotropy as quantified by Ω corresponded to a bias of contact normals in the axial direction. In view of understanding the nature of the stress path ABC, the variations in effective stress components are plotted in Fig. 4. Along AB, the effective axial stress (σ'_1) increases, while the radial one (σ'_3) decreases giving a net decline in mean effective stress p'.

More insight can be gained by plotting the evolution of principal fabric components F_1 and F_3 as seen in Fig. 5 (for 'Fabric' see Satake 1982, Oda 1982, Kantani 1984). Basically, the changes in effective stress components follow those of principal fabric F_1 and F_3. We thus suppose that at the micro/meso-scale, particle redistribution is being made with contact normals realigning themselves along the axial direction at the detriment of contact loss in the radial direction. Based on Figs. 4 and 5, the post snap back at C may be attributed to the loss in confinement and axial support due to fabric reorganization. But the described mechanisms need to be verified, which lead us to the next section.

Observations on Photoelastic Grain Assembly

We study the issue of fabric by loading biaxially a system of photoelastic pentagonal grains, and thereafter observing the particle force chains developed. The study of fabric using photoelastic materials is not new (e.g., Drescher & de-Josselin de Jong 1972, Oda et al. 1980, Geng et al. 2003). Axial and lateral displacement rates ($\dot{D}_1$ and $\dot{D}_2$) are applied in a ratio defined as $\vartheta^* = (\dot{D}_1 + \dot{D}_2)/(\dot{D}_1 - \dot{D}_2)$.

The resulting forces are denoted by f_1 and f_2 respectively. Fig. 6 shows the force response paths for various ϑ^* values, which reveal to be similar to the stress paths previously discussed in triaxial stress conditions (Fig. 2). Here F_d and F_m are the deviatoric and mean forces respectively as a result of $F_d = (f_1 - f_2)/2$ and $F_m = (f_1 + f_2)/2$.

The evolution of axial and lateral forces f_1 and f_2 is shown in Fig. 7 for the path $\vartheta^* = -0.67$ in particular. We observe a quite similar trend as the one described in Fig. 4 for model simulations, in which forces/stresses drop (A-B) and then rise (B-C).

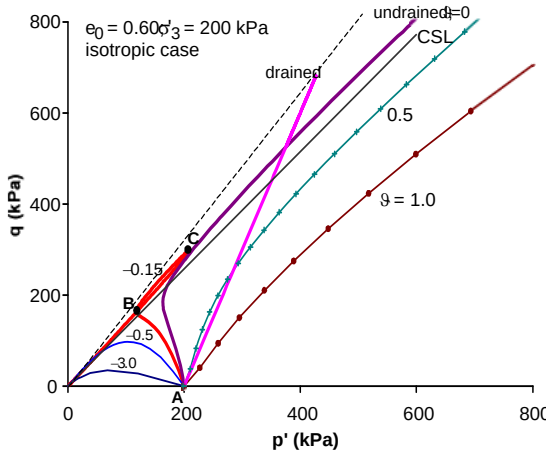

Fig. 2 Effective stress paths for different ϑ values

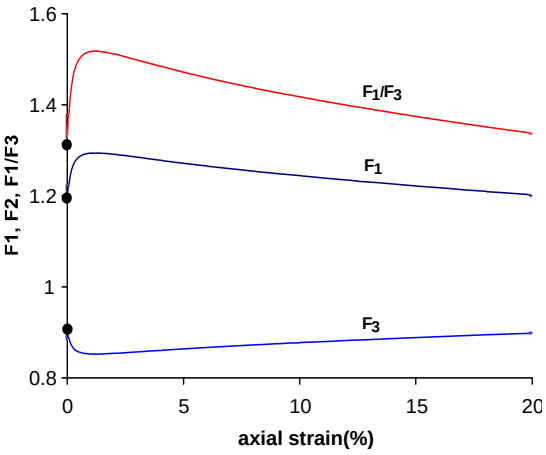

Fig. 5 Evolution of fabric along stress path: $\vartheta = -0.15$

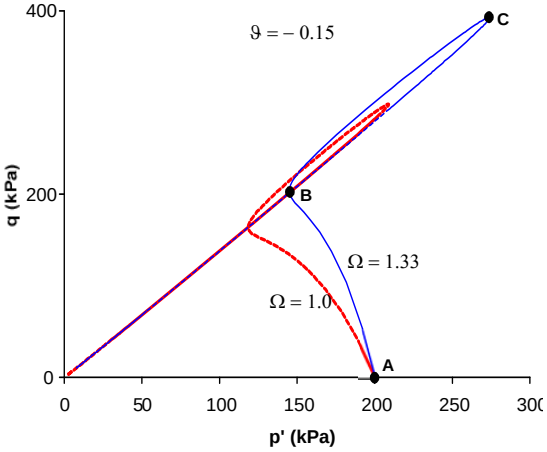

Fig. 3 Effect of fabric on the stress path for $\vartheta = -0.15$

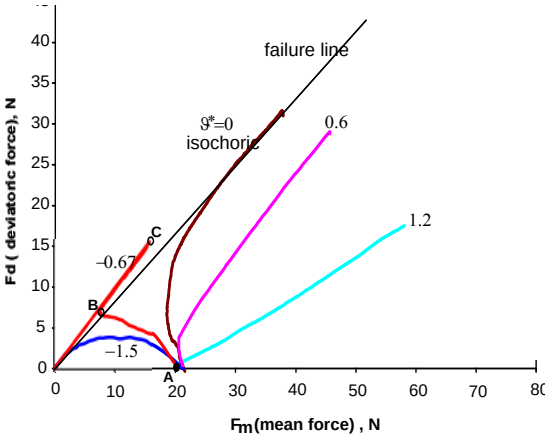

Fig. 6 Force response of photoelastic disk assembly

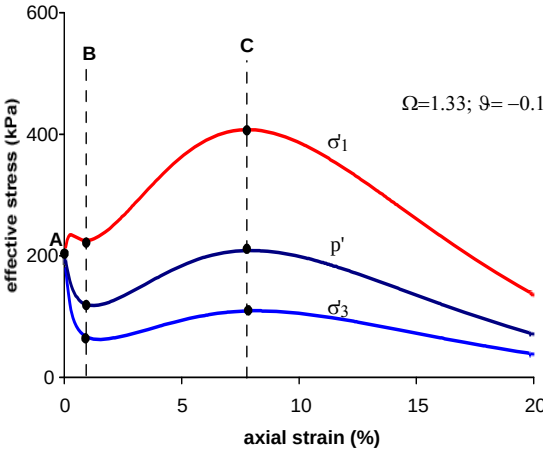

Fig. 4 Evolution of effective stresses: $\vartheta = -0.15$

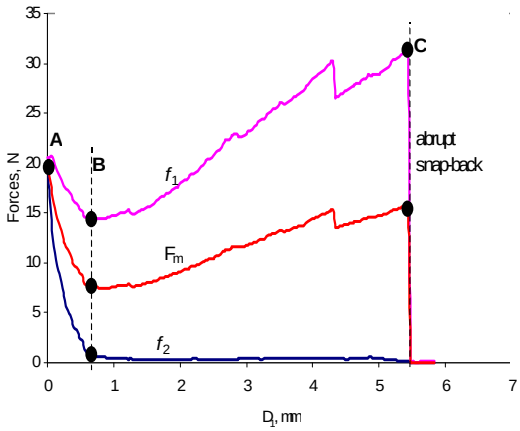

Fig. 7 Force component evolution along path ABC

Fig. 8 reveals the contact force chain and associated structure at key points A, B and C on the force response curve plotted in Fig. 6. The fringe patterns indeed indicate the formation of contact force chains as we move along from A to B leading to a reduction in both axial and lateral loads. Between B and C, additional force chains develop in the axial direction so that the axial load (f_1) picks up. At the same time, in order to sustain the deformation as prescribed by ϑ^*, the lateral load has to decrease so as to allow the required dilation. The force chains ultimately buckle at point C corresponding to the snap back. It is also interesting to note that a two-phase structure emerges with the force chains seen embedded into a matrix of apparently less loaded particles. The mechanism of contact force chain build up and buckling concur with the model simulations presented in the previous section. This suggests that it is possible to describe micro/meso phenomena through a continuum level model with an embedded fabric tensor.

Effect of Micro-Features on Macro Response

Inspired from the observations in the previous section, the experimental modeling was further extended to study the effect of subtle changes in micro features of fabric produced by varying the shape, diameter and packing of the photoelastic grains. Firstly, the pentagonal disks (grains) were changed into circular disks of 7 mm in diameter, the contour of which circumscribed the pentagonal section. It is expected that circular disks are less susceptible than the pentagonal disks to developing fabric due to the smoothness of the disk contour. Secondly, smaller circular disks of 5 mm in diameter were used to further investigate the size issue. For ease of comparison, the deformation rate ϑ^* was kept the same and equal to –0.67 for all the cases studied. Indeed, this provides a unique opportunity to critically investigate microscopic force transmission under different fabrics but the same deformation history. Furthermore, the issue of inherent packing anisotropy was studied for both 5 and 7 mm circular disks, where again the same deformation ratio $\vartheta^* = -0.67$ was maintained with deformation rates $\dot{D}_1$ and $\dot{D}_2$ being interchanged between the two principal directions. If there were no packing anisotropy present in the samples, their response should be identical to each other. But a marked change in behavioral response was observed, which will be reported here.

Effect of Grain Shape

7mm circular disks: In contrast to the pentagonal disk case discussed in the previous sections, both forces F_1 and F_2 steadily decrease throughout deformation history, see Fig. 9a. Fig. 9b. shows the force response path with strategic points A, B, C and D marked down. It is interesting to note that there is no snap back phenomenon occurring as was the case in the pentagonal disk assembly. In order to get more insight in the development of failure mechanism during loading history, the disk packing corresponding to the different stages of the force response path are subsequently given in Figs. 9c, d, e, f. At point B, some disks in the central part of the specimen are highly stressed in comparison with other ones at the two lateral sides. Then as the peak point (point C) on the force response path is reached, a general weakening of the central core occurs, until finally at point D and beyond, the fringes correlating to intensity of contact forces disappear for most of the disks in a diffuse manner. The latter corresponds to a progressive softening of the sample that exacerbates in time to eventually lead to its collapse. It is clear from the images that the sample never hardens in this case, which is in contrast with the pentagonal disk case where the sample showed remarkable hardening until it could no longer hold loads anymore and succumbed to collapse as force chains buckled. In general, it can be concluded that the lack of interlocking between grains weakens the sample significantly.

Effect of Grain Size

5mm circular disks: For same $\vartheta^* = -0.67$ values, images at different points of stress path of 5 mm disk sample is shown in Fig. 10. It is interesting to note that change in diameter significantly changes the response in spite of same packing and void ratio. In this case (5mm disk) quite a bit of sample hardening observed compared to 7 mm disk (Fig. 9). In Fig 10a shows mean stress (F_m) after initial fall remain same for large amount of shearing (from point B to D). In case of 7 mm sample no such response was observed (see Fig. 9a), where mean stress fall all the way down. The change in response for 5 mm disk can be explained from photoelastic images. In images of point B (Fig. 10d) a visible core of highly stressed region is seems to develop in the middle to support increasing stress along vertical direction. With further shearing at point C sample starts to soften where disks along diagonal direction starts to slip with each other and thereby the strong core no longer exists. Once this is initiated, disks slip forming a wedge (as shown in image of point D, Fig. 10f) and sample is unstable afterward.

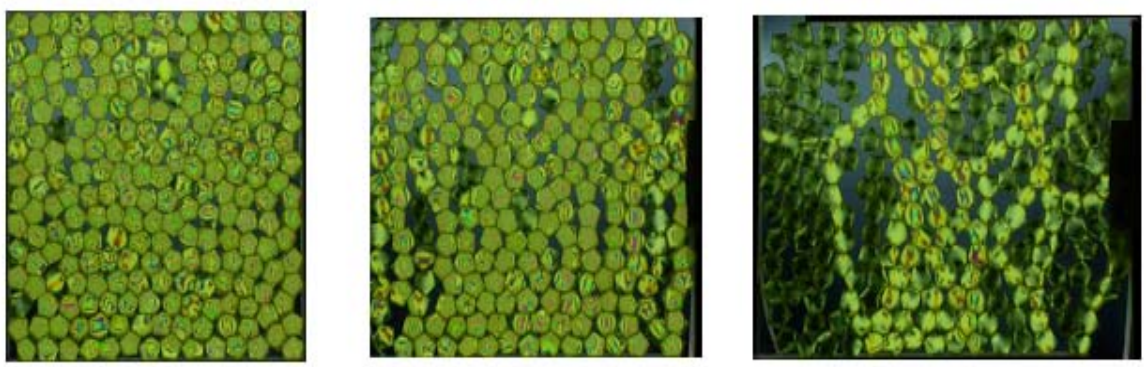

Initially (A) Turning Point (B) Snap-back Point (C)

Fig. 8 Force network developed at key points A,B and C

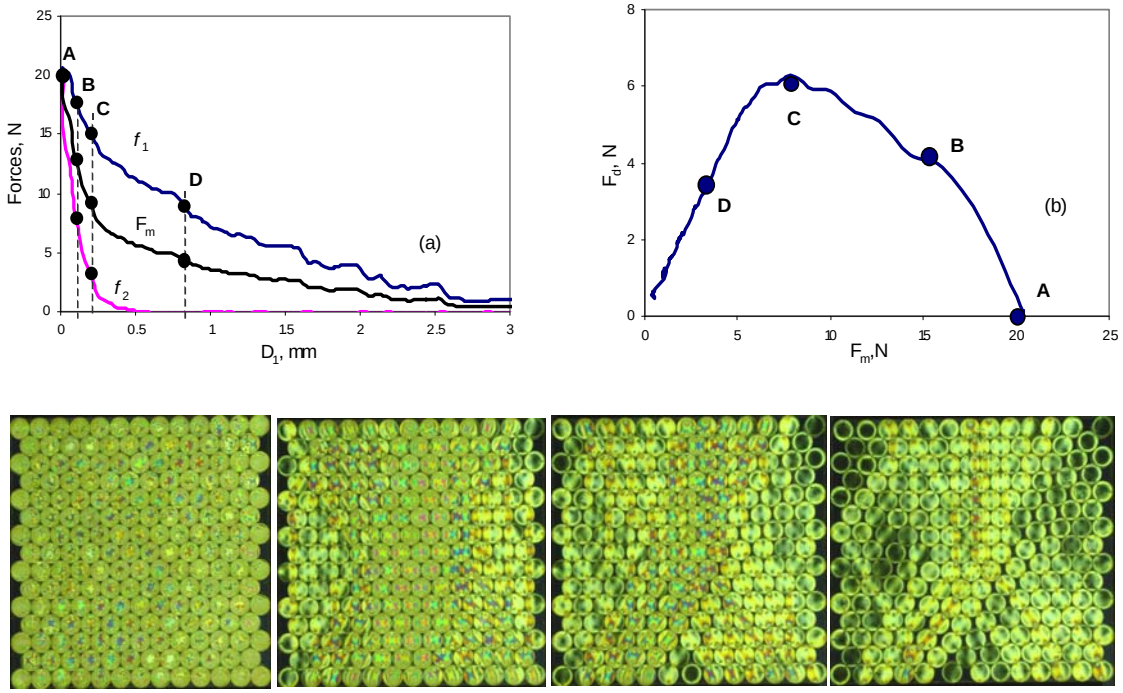

(c) Point A (d) Point B (e) Point C (f) Point D

Fig. 9 Force components, force response path and network at key points for 7 mm circular disks

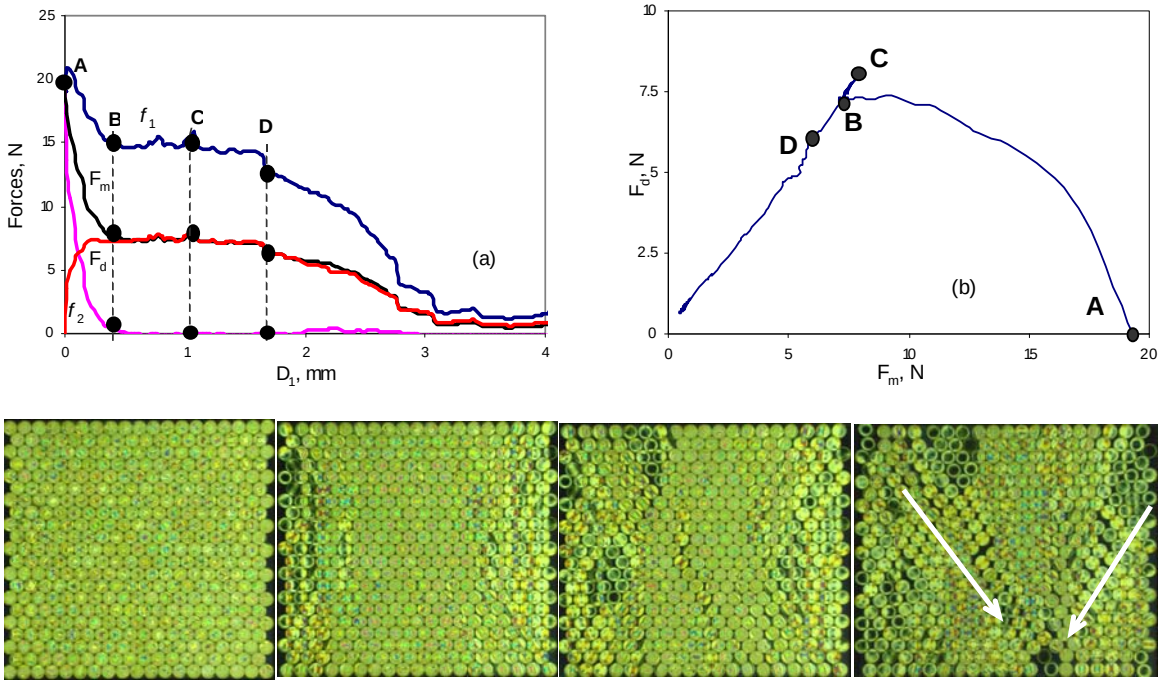

(c) Point A (d) Point B (e) Point C (f) Point D

Fig. 10 Force components, stress path and force network at key points for 5 mm circular disks

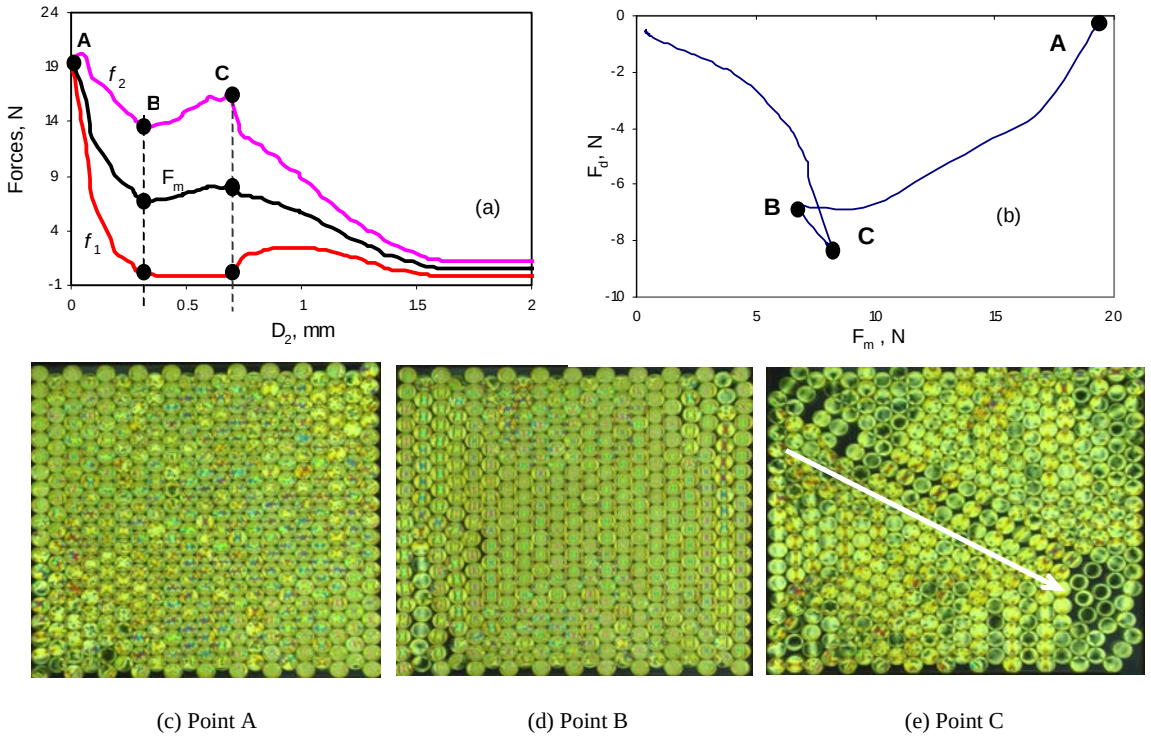

(c) Point A (d) Point B (e) Point C

Fig. 11 Force components, force response path and network at key points for 5 mm circular disks in switched condition

Effect of Anisotropy in Packing

Unlike in pentagonal disks, the packing of circular disks into a dense configuration leads to an incomplete filling, leaving intermittent gaps at the two lateral boundaries as opposed to the top and bottom boundaries of the specimen, see Figs. 9 and 10. This endows the specimen with some inherent anisotropy that has to be investigated. Consequently, deformation rates $\dot{D}_1$ and $\dot{D}_2$ as applied earlier along major (f_1) and minor (f_2) principal directions (vertical and horizontal directions) would result into a different response if these deformation rates were switched between two principal directions. More precisely, this is similar to rotating the principal directions by 90^0. Unlike in the previous cases, the switched deformation rates $\dot{D}_1$ and $\dot{D}_2$ were applied along horizontal and vertical directions respectively for the same imposed dilation rate $\vartheta^* = -0.67$. Notations of forces are kept same such that $\dot{D}_2$ and $\dot{D}_1$ are acting along f_1 and f_2 directions respectively yielding a negative value of F_d in this case as $f_2 > f_1$. Images are shown at a 90^0 rotated (clockwise) position so that the vertical direction is parallel to deformation rate $\dot{D}_1$. This facilitates the comparison of the switched condition with the previous case.

Fig. 11 shows the images of disk packing at several points for 5 mm circular disks when the rate of strains were switched to observe the effect of anisotropy. This reveals a whole different picture indicating a different failure and load transmission mechanism. Unlike in Fig. 10a, the force component f_2 increases (from point B to C) after an initial drop as shown in Fig. 11a. This results into the formation of a small hook in the force response path in Fig. 11b. The force transmission mechanism at point B is shown in Fig. 11d. In this case once shearing was initiated, the disks unlock to form individual columns along vertical directions due to the grain packing structure. Upon further shearing, these columns of disks strengthen so that the force f_2 tends to increase (acting along vertical direction of the images), see Fig. 11a. However, as these columns are slender they cannot sustain higher forces without lateral support. Hence, they start to buckle at some stage of shearing and subsequently lead to failure of the sample. This buckling forms a shear band like structure as shown in Fig. 11e corresponding to point C. Again in this case the sample fails at lower axial displacement compared to previous case (see D_2 at point C in Fig. 11a and D_1 at point D in Fig. 10a). This indicates that the sample is weaker for this switched condition of straining for 5 mm disks.

Similarly, a sample consisting of 7 mm circular disks was also tested for reversed force directions. Images corresponding to several points on the force response path are shown in Fig. 12. From the images (e.g., Fig. 12e) it is clear that the failure mechanism is very similar to that obtained for 5 mm disks. For example, upon shearing individual columns are developed (see image corresponding to point B, Fig. 12d). These columns strengthen further upon shearing, showing some hardening. Subsequently, the columns start to buckle as failure of the specimen is initiated (Fig. 12f). Compared to the 5 mm disk specimen, the one with 7 mm disks failed following the same pattern, but at higher axial deformations. That is, unlike the 5 mm disks, this reverse loading is more stable than the previous condition in Fig. 9. This is due to the larger diameter of the sample. The interesting point is, as grain size is larger, the columns formed are less slender than the one formed by 5 mm disks. Therefore, columns formed of 7 mm circular disks can take more stress without lateral support. Hence for a same void ratio and all around pressure, the grain diameter and packing can significantly influence the response of a granular media under dilation.

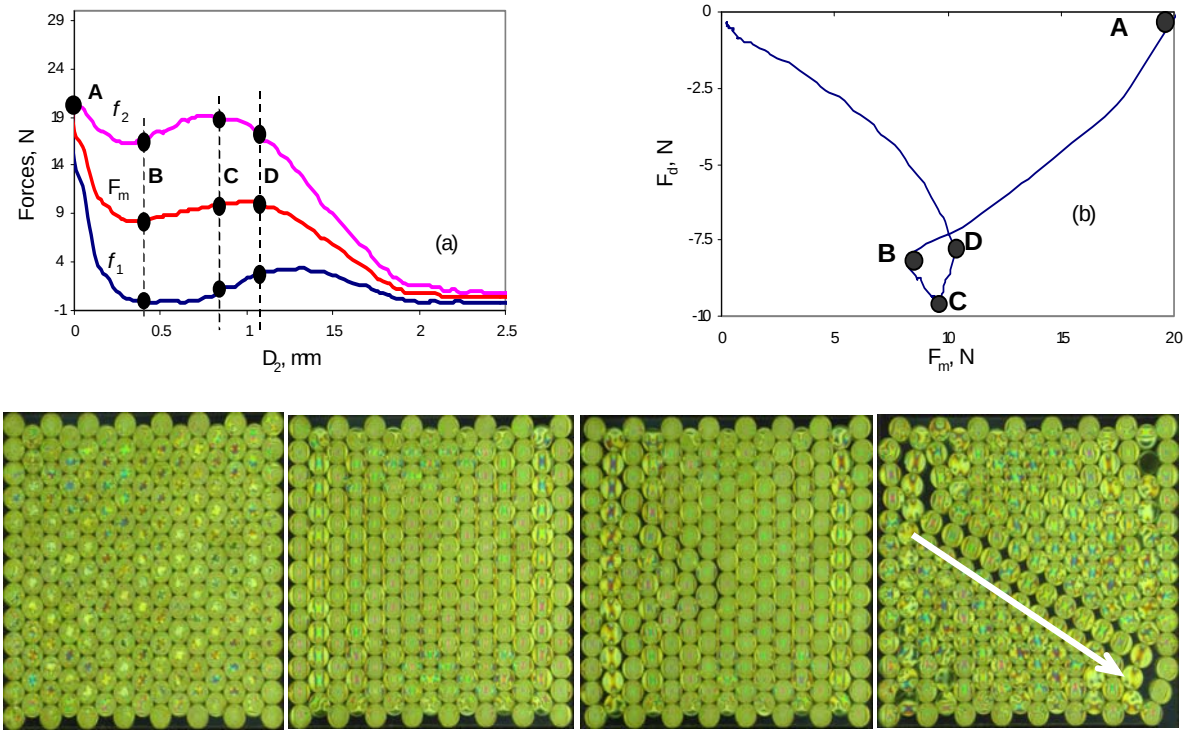

(c) Point A (d) Point B (e) Point C (f) Point D

Fig. 12 Force components, force response path and network at key points for 7 mm circular disks in switched condition.

Conclusion

This study suggests that flow type of failures in soils may not only be restricted to the celebrated saturated loose sand case in undrained conditions. A dense assembly of granular soil will display unstable behavior or subsequently liquefy if loaded along strain paths that involve a particular dilation rate. This dilation rate is also highly dependent on the soil's microstructure. We have demonstrated both numerically and experimentally that fabric, through its kinematical features, plays a dominant role in controlling the macroscopic response of the medium. A fabric dependent stress-dilatancy equation used in the study demonstrates that a continuum elastoplastic model can indeed capture behavioral subtleties of sand response along both stress and strain path histories. Model predictions are confirmed with experimental results obtained in the biaxial testing of photoelastic grains. In such a set-up, forces, displacements, as well as contact force networks can be measured experimentally. When deforming granular materials along imposed dilatancy paths, it is shown that the mechanism of failure corresponds to one in which strong force columns of interconnected particles are initially formed during the hardening phase. Failure then ensues due to the force columns buckling under increased shearing and decreased lateral confinement that are both required to maintain the imposed dilatancy rate. In conclusion, this paper demonstrates experimentally the important role of microstructure in the behavior of granular materials and the possibility of capturing microstructural features using a fabric embedded stress-dilatancy equation. Photoelastic nature of the model granules evolve as an effective tool to critically investigate the microscopic force transmission in a granular mass under complex straining combinations. Changes in fringe pattern with applied strain provide a qualitative measure of fabric evolution at that state of stress. A quantitative measure of the stress field at the point of contact between two neighboring granules from image analysis will give more insight, which is the subject matter of future research.

Acknowledgment

Funding provided by the Natural Science and Engineering Council of Canada is gratefully acknowledged. The photoelastic disk studies were performed within a research project funded by Alberta Innovation and Science.

References

Chu J, Lo S-CR and Lee IK (1992). Strain-softening behavior of granular soil in strain-path testing. *ASCE J. Geotech. Engg*., 118(2), 191-208.

Drescher A and de-Josselin de Jong G (1972). Photoelastic verification of a mechanical model for the flow of a granular material. *J. Mech. Phys. Solids*, 20(5), 337-51.

Geng J, Hartley RR, Howell D, Behringher RP, Reydelley G and Clement E (2003). Fluctuations and instabilities in granular materials. *Bifurcations and Instabilities in Geomechanics, Labuz & Dreschers (eds*), Minnesota, June 2-5, 2002, 79-92.

Guo PJ (2000). Modelling granular materials with respect to stress-dilatancy and fabric: A fundamental approach. *PhD. Thesis*, The University of Calgary, Department of Civil Engineering, 375p.

Hill R (1959). Some basic principles in the mechanics of solids without a natural time. *J. Mech. Phys. Soilds*. 7, 209.

Kantani K (1984). Distribution of directional deta and fabric tensor. *Intl. J. Engg. Sci*., 22(2), 149-64.

Matsuoka H and Takeda K (1980). A stress-strain relationship for granular materials derived from microscopic shear mechanism. *Soils and Foundations*, 20(3), 45-58.

Nemat-Nasser S (2000). A micromechanically-based constitutive model for frictional deformation of granular materials. *J. Mech. Phys. Solids*, 48, 1541-63

Oda M, Konishi J and Nemat-Nasser S (1980). Some experimentally based fundamental results on the mechanical behavior of granular materials. *Geotechnique*, London, UK, 30(4), 479-95.

Oda M (1982). Fabric tensor for discontinuous geological materials. *Soils & Foundations*, 22(4), 96-108.

Oda M and Iwashita K (1999). Mechanics of granular materials. A.A. Balkema, Rotterdam, Netherlands.

Rowe PW (1962). The stress-dilatancy relation for static equilibrium of an assembly of particles in contact. *Proc. of the Royal Society of London*, 269, Series A, 500-27.

Satake M (1982). Fabric tensor in granular materials. *IUTAM Symp. on Deformation and Failure of Granular Materials*, (eds: Vermeer PA & Luger HJ), Rotterdam: Balkema, 63-98.

Vaid YP and Saivathayalan S (2000). Fundamental factors affecting liquefaction susceptibility of sands. *Can. Geotech. J.*, 37, 592-606.

Wan RG and Guo PJ (2001). Drained cyclic behavior of sand with fabric dependence. *ASCE J. Engg. Mech.*, 127(11), 1106-16.